13th International Symposium on Particle Image Velocimetry – ISPIV 2019
Munich, Germany, July 22-24, 2019

Investigation of the 3D Flow in a Combustion Engine using High-Speed Tomo-PIV

Marco Braun[1*], **Wolfgang Schröder**[1], **Michael Klaas**[1]

[1] RWTH Aachen University, Institute of Aerodynamics, Aachen, Germany

[*] m.braun@aia.rwth-aachen.de

Abstract

Due to the worldwide increase in the transportation sector and increasingly strict legal regulations for vehicle emissions, engine manufacturers have to improve engine efficiency, reduce fuel consumption, and lower the level of NO_x and carbon emissions. Therefore, extensive knowledge of the engine flow, which needs to be highly resolved in time and in space, is necessary to further improve engine processes (Heywood (1988); Lumley (1999)). For this purpose, high-speed tomographic particle-image velocimetry (HS-TPIV) measurements are conducted to capture the flow field in a direct-injection spark ignition internal combustion engine for a set of different intake conditions. The measurement results are used to analyze the formation and the spatial and temporal development of the tumble vortex, which is the dominant large-scale flow structure inside most DISI engines, since it is the fundamental mechanism that governs the mixture formation and that conserves energy during the intake and compression stroke. The analysis of the results shows that the average flow velocity is negligibly affected by the intake pressure. However, distinct local effects, i.e., a redistribution of the in-cylinder velocities can be identified.

1 Introduction

The worldwide increase in the transportation sector and the increasingly strict legal regulations for vehicle emissions to alleviate global warming are among the major challenges society and engine manufacturers are facing today. Moreover, the increase in fuel demand leads to a significant decrease in fossil energy reserves and the depletion of global oil reserves was anticipated to 2043 in the literature (Shafiee and Topal, 2009; Singh and Singh, 2012). Therefore, engine researchers aim at significant improvements in combustion processes to reduce engine emissions, i.e., NO_x, CO_2, and soot, and to increase engine efficiency.

All engine combustion concepts of internal combustion engines (ICE) rely significantly on the air-fuel mixture formation, which results from the mixing process during the intake and the compression stroke (Druault et al., 2005; Heywood, 1988; Lumley, 1967). Therefore, engine efficiency, fuel consumptions, and engine emissions correlate directly with the flow during these two strokes. Evidently, extensive fundamental knowledge of the flow is required to generate optimized mixtures of air and fuel for every operating point and combustion concept. In general, the flow topology in internal combustion engines is characterized by time-dependent, highly three-dimensional large-scale coherent flow structures. Direct-injection spark-ignition (DISI) engines usually feature a so-called tumble vortex as the predominant flow structure, while a swirl vortex is used to induce mixing in compression ignition (CI) engines (Borée and Miles, 2014). Additionally, the entire in-cylinder flow topology is affected by cycle-to-cycle variations (CCV). In accordance with Voisine et al. (2010) and Borée and Miles (2014), CCV can be defined as the cycle-dependent fluctuations found in the large-scale coherent flow structures. Since the temporal and spatial development of the large coherent structures and the CCV directly influences the engine performance (Heywood, 1988; Lumley, 1999), fundamental knowledge of the development of the flow field at high spatial and temporal resolution has to be achieved.

Therefore, the scope of this study is the measurement of the three-dimensional and time-dependent flow in an internal combustion engine using high-speed tomographic particle-image velocimetry (HS-TPIV) to achieve spatial and temporal resolutions that allow to investigate the CCV and the coherent flow structures.

2 Experimental Methods

All experiments are performed in an optical research ICE single-cylinder four-valve direct-injection spark-ignition (DISI) engine, custom-made by FEV GmbH, Germany. The engine parameters are listed in tab. 1. The engine possesses a pent roof combustion chamber with two intake and two exhaust valves. The quartz glass cylinder liner features full optical access to the combustion chamber from nearly all directions, since the engine head is positioned on three supporting pillars (fig. 1(a)), and the entire height of the piston stroke can be observed. The predominant coherent flow structure of the in-cylinder flow is a tumble vortex, which is introduced by the engine's tumble intake ports at tumble numbers of approx. $2-4$ depending on the crank angle (CA) (Bücker et al., 2012). Furthermore, the engine is externally driven by a 30 kW electrical engine to remove soot and combustion residues due to fuel combustion from the experiments. The engine is equipped with an oil conditioning system that preheats the engine oil to operating conditions and also heats the entire engine to uniform boundary conditions of approx. 60° C. To realize the different intake pressure levels of 1.0 bar, 1.2 bar, and 1.4 bar, an intake air conditioning system is used, and all measurements are conducted at an engine speed of 1,500 rpm.

Table 1: Parameters of the optical research engine (Braun et al., 2018a; Bücker et al., 2012). atdc/btdc: after/before top dead center

engine parameter	value
bore	75 mm
stroke	82.5 mm
displacement volume	364 cm^3
effective compression ratio	7.4:1
number of valves	4
valve lift	9 mm
intake valve diameter	27.1 mm
exhaust valve diameter	23 mm
intake valves open (1 mm lift)	12° atdc
intake valves close (1 mm lift)	196° atdc
exhaust valves open (1 mm lift)	204° btdc
exhaust valves close (1 mm lift)	20° btdc
connecting rod length	146 mm
crank radius	42.2 mm
oil temperature	$\sim$ 60° C
intake temperature	$\sim$ 20° C
intake pressure	1.0 bar; 1.2 bar; 1.4 bar
max. engine speed	1,500 rpm

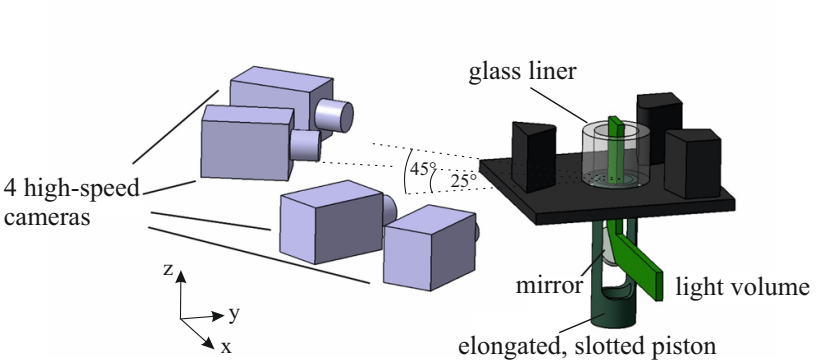

(a) HS-TPIV measurement setup

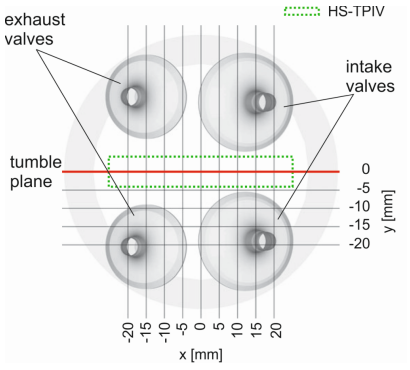

(b) Coordinate system of the engine and measurement volume

Figure 1: (a) HS-TPIV setup at the optical research engine. (b) Coordinate system of the engine cylinder and position of the measurement volume.

The experimental setup to conduct the HS-TPIV measurements is depicted in fig. 1(a). It consists of four high-speed PIV cameras, i.e., two Photron FASTCAM SA5 and two Photron FASTCAM SA3, each equipped with a Tamron 180 mm lens adjusted to a focal number of f/11 under Scheimpflug condition, a Quantronix Darwin Duo 527-100-M (λ = 527 nm) high-speed PIV laser, and laser optics. As depicted in fig. 1(a), the outer cameras (SA5) are set up under an angle of 45° to the normal vector of the measurement volume and the inner cameras (SA3) feature an angle of 25°. The laser is operated at a frequency of 900 Hz per cavity and the laser beam is introduced to the combustion chamber from the bottom using a mirror placed in the prolonged, hollow piston. The laser optics form the laser beam into a measurement volume that is placed in the combustion chamber, centered around the tumble plane, see fig. 1(b). The measurement volume features a width of 50 mm, a depth of 8 mm, and a height depending on the crank angle. At the maximum extension of the combustion chamber, i.e., when the piston is at bottom dead center (bdc), the height of the measurement volume is 83 mm, which covers the entire stroke. Di-Ethyl-Hexyl-Sebacat (DEHS) with a particle diameter of approx. 0.35 - 0.45 µm is used as seeding medium for the PIV measurements. The flow field is captured in steps of 10° crank angle (CA) between 50° atdc and 330° atdc for more than 200 engine cycles using a pulse distance of 30 µs at a pulse energy of approx. approx. 30 mJ per cavity. All relevant parameters of the HS-TPIV measurements and their processing are listed in tab. 2.

Table 2: Parameters of the setup and the processing of the HS-TPIV measurements

parameter	value
seeding particles	Di-Ethyl-Hexyl-Sebacat (DEHS)
particle diameter	$\sim$ 0.35 - 0.45 µm
laser	Darwin Duo 527-100-M
laser wavelength	527 nm (Nd:YLF)
laser frequency	900 Hz per cavity
laser pulse energy	$\sim$ 30 mJ/cavity (without losses)
temporal resolution	10° CA
crank angle regime	50 - 330° atdc
measurement volume	$\sim$ 50x8x83 mm^3
pulse distance	30 µs
cameras (inner)	2x Photron Fastcam SA3
cameras (outer)	2x Photron Fastcam SA5
viewing angle (SA3)	$\pm$ 25°
viewing angle (SA5)	$\pm$ 45°
lens	Tamron 180 mm macro
lens aperture	f/11
magnification	$\sim$ 0.2
sampled images	225 cycles, 29 image pairs each
interr. box (initial)	80x80x80
interr. box (final)	32x32x32 px^2 @ 75 % overlap
vector spacing	8 vox $\approx$ 0.67 mm

For the calibration, a transparent single-plane calibration target is recorded by all camera views in five co-planar, equidistant calibration planes. The transformation matrix is calculated for each calibration plane using a 3rd order polynomial utilizing all four views, in-between interpolation is utilized. To further improve the transformation matrix and to reduce the deviation of the disparity to below 0.48 pixels, volume self calibration is applied. The pre-processing of the particle images includes masks, a sliding time filter, subtraction of a 5x5 sliding minimum, and a 3x3 Gaussian smoothing algorithm to further improve the quality of the particle images. Subsequently, the fast-MART algorithm is used for the volumetric reconstruction with seven iterations and smoothing steps in-between. The maximum measurement volume of 50x8x83 mm^3 is reconstructed to a size of 901x997x97 voxels^3 with a resolution of approx. 0.083 mm/vox. A direct multi-pass correlation with five correlation box steps between the initial box size of 80x80x80 voxels^3 and the final box size of 32x32x32 voxels^3 yields a vector spacing of 8 voxels and 0.67 mm, at 75 % vector overlap. Between the correlation steps, three 5x5x5 universal outlier detection steps as well as five 3x3x3 smoothing steps are conducted. The flow field post-processing and the calculation of the flow quantities are performed as in Braun et al. (2018b). Furthermore, an extensive validation, a discussion of the measurement quality, and an investigation of instantaneous engine cycles can be found in Braun et al. (2019b).

3 Results

Figure 2 shows the temporal development of the ensemble- and volume-averaged kinetic and turbulent kinetic energy for the three intake pressures of 1.0 bar, 1.2 bar, and 1.4 bar at an engine speed of 1,500 rpm. During the early intake stroke, both volume-averaged quantities start at very high values at 50° atdc. For this crank angle range, the extension of the combustion chamber is very small and the flow in the cylinder is dominated by the highly turbulent, high velocity flow through the small gaps of the intake valves. As the piston moves downward, i.e., as the extension of the combustion chamber increases, the impact of the intake jets on both volume-averaged energy distributions is reduced, which leads to local minima of both quantities at approx. 70° atdc for all three intake pressures. The increasing valve lift, which reaches its maximum at approx. 100° atdc, and the high piston velocity, which is maximum at approx. 90° atdc, cause an increase of the kinetic and the turbulent kinetic energy up to a crank angle of approx. 90-100° atdc. Subsequently, the piston velocity decreases, the size of the combustion chamber increases towards its maximum volume, and the inlet valves start to close. Hence, both energies decrease gradually until they reach their minimum at the end of the first half of the compression stroke. During the second half of the compression stroke, the so-called tumble spin-up process is induced. The tumble vortex is pushed towards the pent roof and the kinetic energy increases significantly. At approx. 280° atdc, the turbulent tumble break-up process is initialized. The large-scale coherent vortical flow structure starts to dissolve into turbulent small-scale vortical structures and the turbulent kinetic energy in the flow increases significantly. In fired engine operation, this high level of turbulence is required for a good combustion performance.

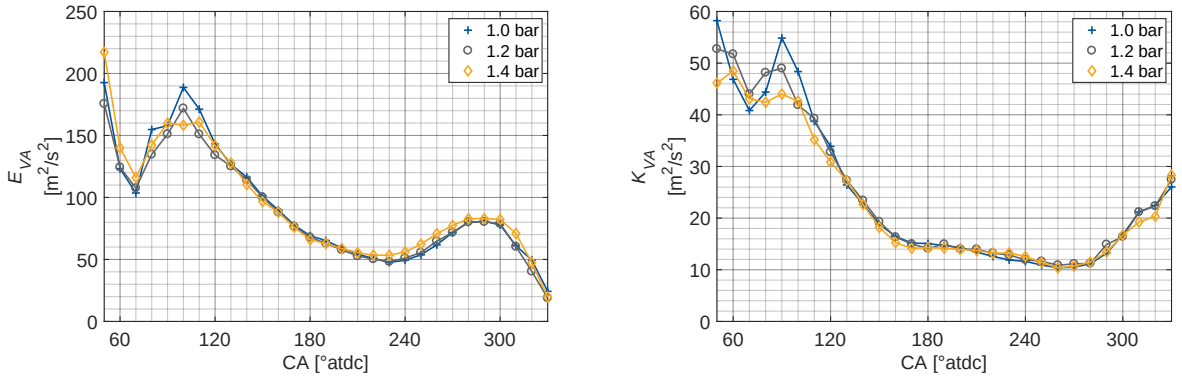

(a) Kinetic energy

(b) Turbulent kinetic energy

Figure 2: Temporal evolution of the volume- and ensemble-averaged kinetic and turbulent kinetic energy for three intake pressures of 1.0 bar, 1.2 bar, and 1.4 bar at an engine speed of 1,500 rpm. Adapted from Braun et al. (2019a).

A variation of the intake pressure possesses only a minor influence on the temporal evolution of the energy distributions. The highest intake pressure goes along with the highest kinetic energy in the second half of the compression stroke, however, the difference in the overall values for all three inlet pressures is within the standard deviation of the measurements. Noticeable deviations only can be seen around 90° atdc and 100° atdc, where significant fluctuations due to turbulence and CCV can be found. Nonetheless, those differences vanish completely within the next approx. 20-30° CA.

The tumble vortex is a key factor for the generation of the mixture of fuel and air in the cylinder. Figure 3 shows its ensemble-averaged trajectory, which is derived from the locations of the core of the tumble vortex in the ensemble-averaged flow fields of all investigated CA locations. The position of the vortex core is determined according to Graftieaux et al. (2001) using the extrema of the scalar Γ_1-function. The trajectory begins at approx. 70° atdc where the vortex starts to evolve in the combustion chamber. The tumble vortex moves towards the center of the combustion chamber until approx. 100° atdc and then shifts towards the right side of the chamber. It follows the piston until reaching its most downward position in the cylinder at 160° atdc, before it starts to move towards the opposite side of the combustion chamber. After 200° atdc, the vortex is rapidly pushed towards the top left area of the cylinder, where it is located until approx. 260° atdc. Finally, the tumble vortex moves towards the right hand side of the combustion chamber where it dissolves near the pent roof. The different intake pressures show only minor differences in the tumble trajectory.

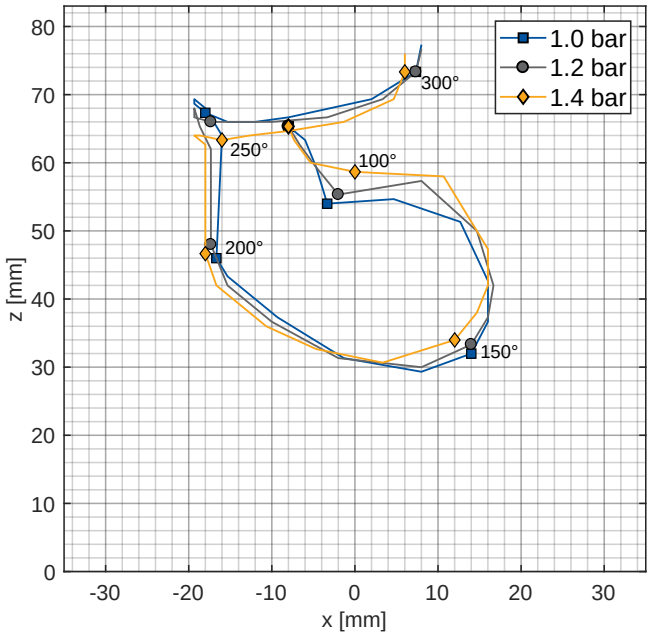

Figure 3: Ensemble-averaged temporal trajectory of the core of the tumble vortex through the combustion chamber during the intake and the compression phase. The position of the tumble vortex core is determined using the Γ_1-criterion. Adapted from Braun et al. (2019a).

However, the increase in intake pressure leads to a more-well rounded and more circular path of the tumble vortex core in the combustion chamber.

Figures 2 and 3 show that the intake pressure possesses only aminor influence on the volume-averaged energies and on the tumble trajectory and, hence, on the flow field on a global scale. However, this does not necessarily mean that the influence of the inlet pressure on the flow on a local scale can also be considered negligible. Fig. 4 shows the three-dimensional in-cylinder flow structures for three selected CA and for the highest and lowest intake pressure, i.e., 1.0 bar and 1.4 bar, to analyze the local effect of the intake pressure on the engine flow. The figure juxtaposes the three-dimensional distributions of the in-cylinder velocity magnitude (isosurfaces) $U_{mag} = \sqrt{u_{EA}^2 + v_{EA}^2 + w_{EA}^2}$ and the ensemble-averaged velocity vectors in the tumble plane (arrows).

At 100° atdc (fig. 4(a) and 4(b)), i.e., during the early phase of the intake stroke, the flow field is dominated by the high velocity of the intake jets for both intake pressures. The isosurfaces for $U_{mag} = 8\,\mathrm{m/s}$ near the center show that a well-defined tumble vortex has formed. The comparison of the two different intake pressure levels shows a redistribution of the velocities in the cylinder. For an intake pressure of 1.4 bar, the bottom left area of the combustion chamber and the intake jets both feature increased velocities and the intake jets are directed less towards the left side of the cylinder. In contrast, the velocity in the top right corner of the cylinder is reduced and the center of the tumble vortex appears to be more distinct. As found in the kinetic energy in fig. 2(a), the average in-cylinder velocity is reduced for 1.4 bar. However, 100° atdc was identified as the CA location that features the highest difference in the volume-averaged velocities and the majority of the CA locations show only negligible velocity differences.

Towards the end of the intake stroke, i.e., at 160° atdc (fig. 4(c) and 4(d)), the intake jets start to diminish due to the closing intake valves and only small remnants, indicated by the isosurface for $U_{mag} = 20\,\mathrm{m/s}$, remain. The tumble vortex, which is close to the bottom of the combustion chamber at this crank angle, features a significantly larger low velocity region around its core for a higher intake pressure.

Towards the end of the compression stroke, the tumble vortex is compressed pushed towards the pent roof by the upward moving piston. Like at the previous crank angles, the flow fields at 270° atdc again display a redistribution of the velocity inside the combustion chamber as a function of the intake pressure level. For a higher intake pressure, the size of the core region of the tumble vortex is increased further, compared to the earlier crank angle locations.

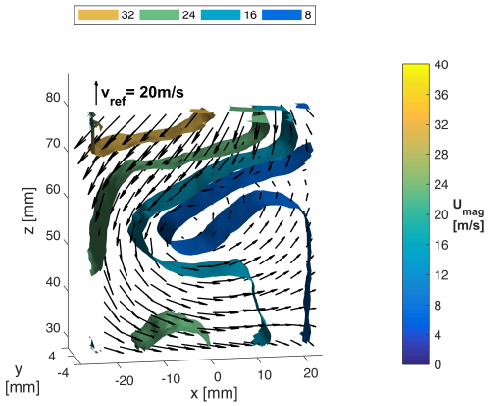

(a) 100° atdc, 1.0 bar

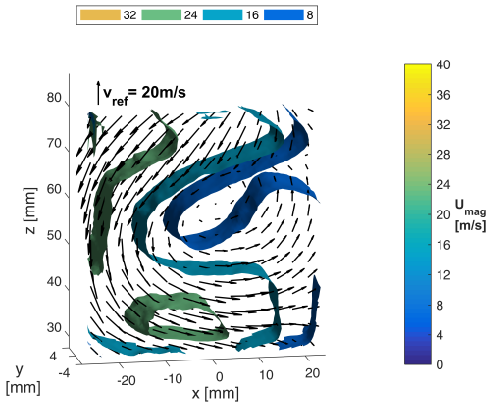

(b) 100° atdc, 1.4 bar

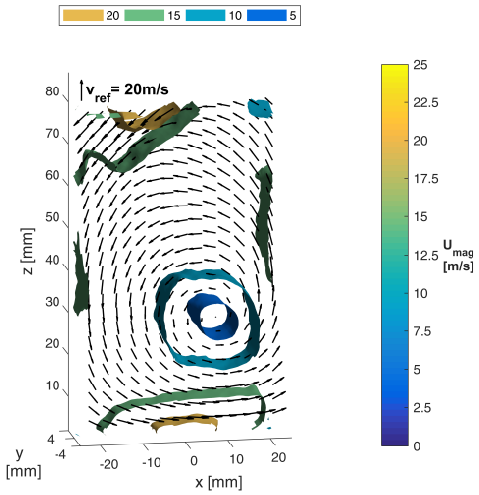

(c) 160° atdc, 1.0 bar

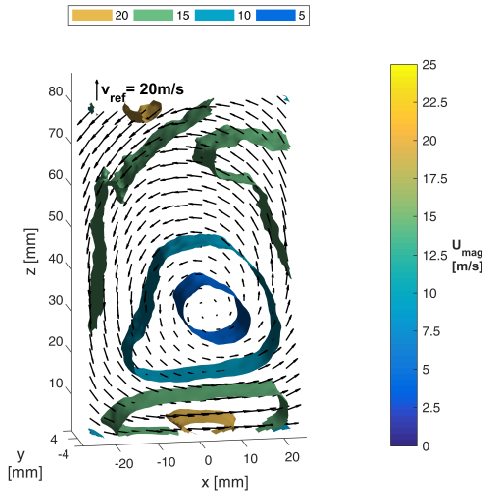

(d) 160° atdc, 1.4 bar

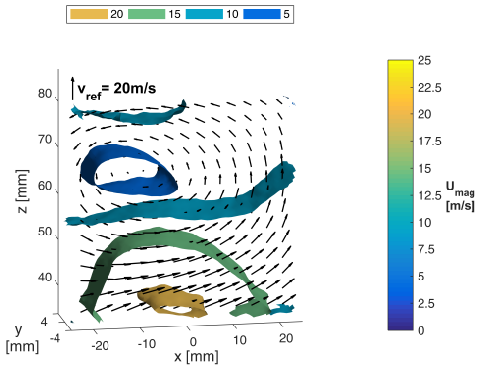

(e) 270° atdc, 1.0 bar

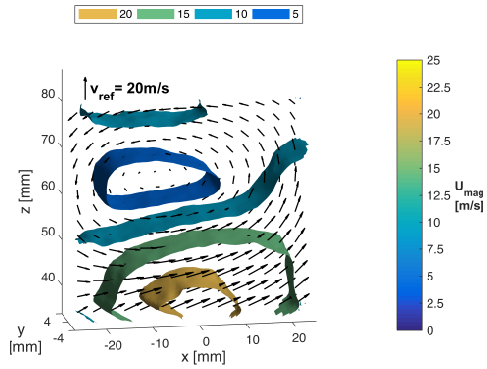

(f) 270° atdc, 1.4 bar

Figure 4: Ensemble-averaged three-dimensional distribution of the velocity magnitude (isosurfaces) and velocity vectors (arrows) in the tumble plane at an engine speed of 1.500 rpm.

4 Conclusion

High-speed tomographic particle-image velocimetry measurements were conducted in an optical DISI research engine for three different intake pressures to analyze the effect of the intake pressure on the in-cylinder flow field. The volume-averaged energies in the cylinder showed the temporal development of the global parameters of the in-cylinder flow. The comparison of the different intake pressures showed that the intake pressure has a more-or-less insignificant impact on the global scale of the in-cylinder flow, especially after approx. 100° atdc. In the discussion of the temporal trajectory of the tumble vortex core through the combustion chamber, a smoothing effect of the intake pressure on the trajectory could be reported. The tumble vortex is more pronounced, larger, and moves more smoothly through the combustion chamber for a higher intake pressure. Although the volume-averaged velocities in the engine cylinder are mostly unaffected by the intake pressure, a distinct velocity redistribution was found.

Acknowledgements

Funded by the Deutsche Forschungsgemeinschaft (DFG, German Research Foundation) under Germany's Excellence Strategy – Cluster of Excellence 2186 "The Fuel Science Center" - ID: 390919832. Furthermore, this research is part of the project "Analysis of cycle-to-cycle variations in IC engines using highspeed Tomographic Particle-Image Velocimetry" funded by the German Research Association (Deutsche Forschungsgemeinschaft, DFG).

References

Borée J and Miles PC (2014) In-cylinder flow. *Encyclopedia of Automotive Engineering*

Braun M, Klaas M, and Schröder W (2018a) Influence of miller cycles on engine air flow. *SAE International Journal of Engines* 11:161–178

Braun M, Klaas M, and Schröder W (2019a) High-speed 3D measurements of the influence of intake pressure on the in-cylinder flow in a DISI engine. in *JSAE/SAE PFL International Meeting*. Kyoto, Japan. (August 26-29, 2019)

Braun M, Schröder W, and Klaas M (2018b) High-speed tomographic PIV in an IC engine. in *19th International Symposium on Applications of Laser Techniques to Fluid Mechanics, Lisbon, Portugal*

Braun M, Schröder W, and Klaas M (2019b) High-speed tomographic PIV measurements in a DISI engine. *Experiments in Fluids* (submitted April 2019)

Bücker I, Karhoff DC, Klaas M, and Schröder W (2012) Stereoscopic multi-planar PIV measurements of in-cylinder tumbling flow. *Experiments in Fluids* 53:1993–2009

Druault P, Guibert P, and Alizon F (2005) Use of proper orthogonal decomposition for time interpolation from PIV data. *Experiments in Fluids* 39:1009–1023

Graftieaux L, Michard M, and Grosjean N (2001) Combining PIV, POD and vortex identification algorithms for the study of unsteady turbulent swirling flows. *Measurement Science and Technology* 12:1422

Heywood JB (1988) *Internal combustion engine fundamentals*. McGraw-Hill, New York

Lumley JL (1967) The structure of inhomogenous turbulent flows. in *Atmospheric Turbulence and Radio Wave Propagation*. pages 166–178. Nauka, Moskau

Lumley JL (1999) *Engines: An Introduction*. Cambridge University Press

Shafiee S and Topal E (2009) When will fossil fuel reserves be diminished?. *Energy policy* 37:181–189

Singh BR and Singh O (2012) *Global Trends of Fossil Fuel Reserves and Climate Change in the 21st Century*. InTech

Voisine M, Thomas L, Borée J, and Rey P (2010) Spatio-temporal structure and cycle to cycle variations of an in-cylinder tumbling flow. *Experiments in Fluids* 50:1393–1407